Xiaowu Zhang[1]
Department of Mechanical Engineering,
University of Michigan,
Ann Arbor, MI 48109
e-mail: xiaowuz@umich.edu

Shengbo Eben Li
State Key Laboratory of Automotive
Safety and Energy,
Tsinghua University,
Beijing 100084, China;
Department of Mechanical Engineering,
University of California, Berkeley,
Berkeley, CA 94720

Huei Peng
Department of Mechanical Engineering,
University of Michigan,
Ann Arbor, MI 48109;
State Key Laboratory of Automotive
Safety and Energy,
Tsinghua University,
Beijing 100084, China

Jing Sun
Department of Naval Architecture
and Marine Engineering,
University of Michigan,
Ann Arbor, MI 48109

Efficient Exhaustive Search of Power-Split Hybrid Powertrains With Multiple Planetary Gears and Clutches

Planetary gear (PG) power-split hybrid powertrains have been used in producing hybrid and plug-in hybrid vehicles from the Toyota, General Motor, and Ford for years. Some of the most recent designs use clutches to enable multiple operating modes to improve launching performance and/or fuel economy. Adding clutches and multiple operating modes, however, also increases production cost and design complexity. To enable an exhaustive but fast search for optimal designs among a large number of hardware configurations, clutch locations, and mode selections, an automated modeling and screening process is developed in this paper. Combining this process with the power-weighted efficiency analysis for rapid sizing method (PEARS), an optimal and computationally efficient energy management strategy, the extremely large design space of configuration, component sizing, and control becomes feasible to search through. This methodology to identify optimal designs has yet to be reported in the literature. A case study to evaluate the proposed methodology uses the configuration adopted in the Toyota Hybrid Synergy (THS-II) system used in the Prius model year 2010 and the Hybrid Camry. Two designs are investigated to compare with the simulated Prius design: one uses all possible operating modes; and the other uses a suboptimal design that limits the number of clutches to three. [DOI: 10.1115/1.4031533]

Keywords: hybrid vehicles, optimal control, planetary gear, optimal design

1 Introduction

The hybrid electric powertrain is one of the most important technologies that have been developed to satisfy the challenging fuel economy standards set by the EU and U.S. Governments [1]. According to a report from the Electric Drive Transportation Association (EDTA), hybrid and electric car sales in 2012 increased by 73% compared with the previous year. Over 473,000 hybrids and plug-in hybrids were sold, representing 3.3% of the U.S. market, a significant increase from the 2.2% share in 2011.

The powertrain system can be made more efficient by using electric motor/generators (MGs). With MGs, the engine can be right-sized to improve efficiency. In addition, MGs enable the use of regenerative braking, which can significantly help fuel economy, particularly in city driving. In terms of the power flow between the engine and the MGs, three types of hybrid vehicles are traditionally available: series, parallel, and series–parallel (power-split) [2,3].

In series hybrids, all the engine power is first converted to electrical power and then back to mechanical form. Excess electrical power is stored in the battery for later use. The multiple stages of energy conversion make series hybrids inherently inefficient, which is the major reason that no production pure series hybrid passenger vehicles are available in the market from major original equipment manufacturers except the BMW i3, a range-extender plug-in hybrid vehicle. However, series hybrid mode can be used as a back-up mode to achieve drivability requirements, as the Chevrolet Volt does [4].

Parallel hybrids can be designed as an incremental add-on to traditional powertrains and thus incur a relatively small investment and effort. Their efficiency in highway driving can be better than the series hybrid since both the engine and the MG can provide torque directly to the wheels without involving extra steps of energy conversion, thereby reducing energy losses. However, the mechanical coupling between the engine and wheels through the transmission makes it hard for the engine to consistently operate in the sweet spot [3].

Among all the strong hybrid vehicle sales in 2012, over 90% were of the power-split type [5], which utilizes one or more PGs as the transmission device. The Toyota Prius, Ford Fusion, and Chevrolet Volt are all power-split hybrid vehicles. The PGs are compact, efficient, and have a high torque capacity. In addition, when the MGs are properly controlled, the PG system performs as an electric continuous variable transmission which can result in efficient engine operation. However, due to the unavoidable energy conversion from the generator to the motor, the power-split vehicles can have greater energy losses compared to parallel hybrid electric vehicles (HEVs) in highway driving.

Using clutches in a power-split powertrain produces different operating modes, thus adding flexibility to vehicle operations. For example, the input-split mode can be used for better launching performance; the compound-split mode can be used for better high-speed driving, while curtailing the operating speed of the electric machines [6]. It is also possible to have parallel modes, series modes, pure electric vehicle (EV) modes, and fixed-gear modes on the same powertrain [7,8]. Having a diverse set of operating modes makes it possible to fully realize the potential of the powertrain and achieve both better fuel economy and improved drivability, as compared to conventional vehicles and traditional hybrid vehicles.

Although many multimode hybrid vehicle configurations and designs have been patented and some implemented commercially [9–12], many more remain unexplored. "Configuration" in this paper refers to the way the power devices (engine and generator/motors) and output shaft are connected to the nodes of PGs, while

[1]Corresponding author.

Contributed by the Dynamic Systems Division of ASME for publication in the Journal of Dynamic Systems, Measurement, and Control. Manuscript received January 5, 2015; final manuscript received August 21, 2015; published online September 23, 2015. Assoc. Editor: Junmin Wang.

"design" in this paper stands for the specific clutch combination for a particular configuration. An exhaustive analysis of all possible configurations and designs has already been conducted for power-split vehicles using a single PG [13]. For power-split vehicles using more than one PG, a general modeling method has been developed [14]. General clutch allocation and identification of unique modes for double PGs were discussed by us in Ref. [15], with an automated modeling methodology proposed and unique modes identified. In this paper, the automated modeling and unique mode identification methodologies are generalized to powertrain systems with more than two PGs.

Once a particular configuration is selected and all the feasible modes are identified, we can use optimal control methods to find the best possible fuel economy for that configuration. For example, in this paper we study the THS-II configuration, which connects the engine, two motors, and the vehicle to the two PGs in a particular way. In addition, two "permanent clutches" are used in the THS-II design. Because the two "clutches" never change state, there is a single operating mode. Our methodology will answer the following four questions: How many clutches can be added and how many distinct modes can be created? Among all possible modes enabled by these clutches, how many of them are useful? If we limit ourselves to no more than three clutches, where should they be located? And for the "enhanced THS-II" (by having either all possible modes or the modes only through three clutches), how much better is the fuel economy compared with the original THS-II?

If fuel economy is the main design objective, the near-optimal control problem can generally be solved using load leveling [16,17], equivalent consumption minimization strategy (ECMS) [18,19], the Pontryagin's minimum principle (PMP) [20–22], dynamic programming (DP) [22,23], and convex optimization [24–27]. The load leveling methods are heuristic and cannot guarantee optimality. ECMS is an instantaneous optimization method but the equivalent fuel consumption factor needs tuning. DP is optimal, but its computation load grows exponentially with the number of state and input variables, a well-known phenomenon commonly referred as "curse of dimensionality." PMP frequently suffers from numerical convergence problems if the underlying two-point-boundary-value problem is nonlinear. While the convex optimization is fast, it cannot address integer decisions, such as mode selection and engagement of clutches.

To overcome these drawbacks, a new near-optimal energy management strategy named PEARS was developed, which has proved to produce optimal results similar to traditional DP but over 3–4 orders of magnitude faster [28]. In this paper, the PEARS method is further enhanced. Rather than using instantaneous optimization, the enhanced PEARS adopts a low-dimension DP to achieve an optimal mode shift schedule and address mode shift feasibility globally. This method is used to generate optimal control results necessary for identifying the best clutch locations and optimal operating modes.

The paper is organized as follows: In Sec. 2, we illustrate the dynamics of the PG system and present an automated modeling procedure as well as a way to screen the modes (to eliminate/identify infeasible and redundant ones) and an identification process for multiple PG systems. Section 3 describes the concept of the PEARS method and its enhancement. In Sec. 4, the configuration of THS-II is the focus of a case study. Section 5 presents conclusions.

2 Dynamics of PG and Automatic Modeling

A PG system consists of a ring gear, a sun gear, and a carrier with several pinion gears. The lever analogy [29] can be applied to reflect the two degrees-of-freedom (DOF) dynamics of this single PG, as shown in Fig. 1. The rotational speeds and accelerations of the three nodes (sun gear, ring gear, and carrier) must satisfy the constraint shown in Eq. (1), where the subscripts s, r, and c indicate the sun gear, ring gear, and the carrier, respectively. S and R are the radii of the sun gear and ring gear

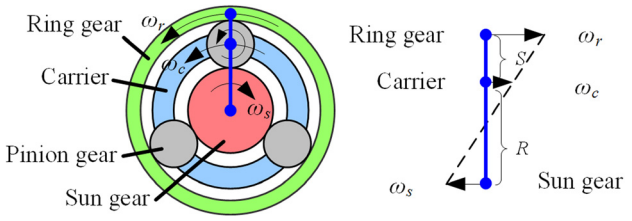

Fig. 1 PG and its lever analogy

$$\omega_s S + \omega_r R = \omega_c (R + S) \tag{1}$$

The dynamics of the PG system can be represented using the state-space form as suggested in Ref. [14]. In this paper, a more general form of the modeling is presented, with all possible clutch locations and modes considered.

2.1 Multiple PG System. Many of today's popular power-split hybrid vehicles use two MGs to enhance the engine efficiency. In this research, we adopt this general powertrain setup. Assuming no component collocation at any of the PG nodes, the number of different configurations ($n_{\text{configuration\_total}}$) and the maximum number of clutches ($n_{\text{clutch\_total}}$) can be calculated by Eqs. (2) and (3), where C_{3n}^{k} is the k-combination and n is the number of PGs. The first term in Eq. (3) stands for the number of clutches that can be added between any pair of nodes in the PGs system, while the second term represents the number of grounding clutches. The third term is the number of redundant clutches that can be eliminated from the system: for each PG, locking any two nodes makes all three nodes rotate at the same speed, which means that only one such clutch is needed. In addition, the grounding clutch for the vehicle output shaft is meaningless during driving, leading to the last term of Eq. (3)

$$n_{\text{Configuration\_total}} = C_{3n}^{4} \tag{2}$$

$$n_{\text{clutch\_total}} = C_{3n}^{2} + 3n - 2n - 1 = C_{3n}^{2} + n - 1 \tag{3}$$

As an example, the diagram of a double PG system is presented in Fig. 2, where up to 16 clutches can be added and the removed clutches are marked in red (assuming the vehicle output is on the second ring gear).

To avoid redundant designs and to facilitate the systematic, automated modeling procedure, an assumption is made that *any* one node can only be connected to no more than two nodes of the other PG at the same time, as the additional connection is redundant.

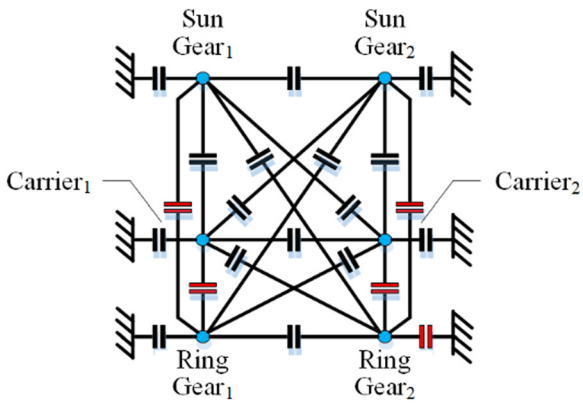

Fig. 2 All 16 possible clutch locations for a double PG system

2.2 Automated Modeling. In this subsection, the automated modeling process for multiple PGs is described.

2.2.1 Step 1: Initialize the A_0 Matrix. The dynamics of the system without any connection can be represented by Eq. (4), where T_0 is the component torque, $\dot{\Omega}$ is the angular acceleration of the powertrain components/PG nodes, and $\dot{\Omega}_0$ is the generalized acceleration vector. A_0 is a $4n \times 4n$ matrix and n is the number of PGs. A_0 can be decomposed into four parts: J is a diagonal matrix with a dimension of $3n \times 3n$, reflecting the inertia of the system. The first four elements of the principal diagonal of J are replaced by the inertias of the powertrain components (i.e., the vehicle, engine, MG1, and MG2) plus the inertia of the nodes they are connected to. In addition to the powertrain components, the other diagonal terms in J are filled with the nodes that are not assigned to any powertrain components, in the sequence of the ring gear, the carrier, and the sun gear, from the first PG to the last PG

$$A_0\dot{\Omega}_0 = \begin{bmatrix} \boldsymbol{J} & \boldsymbol{D} \\ \boldsymbol{D}^{\mathrm{T}} & 0 \end{bmatrix} \begin{bmatrix} \dot{\Omega} \\ \boldsymbol{F} \end{bmatrix} = \begin{bmatrix} \boldsymbol{T} \\ 0 \end{bmatrix} = T_0 \tag{4}$$

The connections of the PG nodes with the four components determine the entries of the upper-right $3n \times n$ constraint matrix D and D^{T} on the bottom-left. Those two matrices are associated with the internal force F_i between the gear teeth, and the number of columns of D is equal to the number of PGs. When one powertrain component is connected to a PG node, the "node coefficients" $-S_i$, $-R_i$, and $R_i + S_i$ will be entered in the corresponding entry in the D matrix if it is connected to the sun gear, ring gear, and carrier of the ith PG, respectively. The remainder of the entries in the D matrix will be filled with zeros.

An example for the configuration used in THS-II (Prius model year 2010) is shown in Fig. 3, whose corresponding matrices are given in the below equation

$$A_0 = \begin{bmatrix} I_{\mathrm{out}} + I_{r2} & 0 & 0 & 0 & 0 & 0 & 0 & -R_2 \\ 0 & I_e + I_{c1} & 0 & 0 & 0 & 0 & R_1 + S_1 & 0 \\ 0 & 0 & I_{\mathrm{MG1}} + I_{s1} & 0 & 0 & 0 & -S_1 & 0 \\ 0 & 0 & 0 & I_{\mathrm{MG2}} + I_{s2} & 0 & 0 & 0 & -S_2 \\ 0 & 0 & 0 & 0 & I_{r1} & 0 & -R_1 & 0 \\ 0 & 0 & 0 & 0 & 0 & I_{c2} & 0 & R_2 + S_2 \\ 0 & R_1 + S_1 & -S_1 & 0 & -R_1 & 0 & 0 & 0 \\ -R_2 & 0 & 0 & -S_2 & 0 & R_2 + S_2 & 0 & 0 \end{bmatrix} \tag{5}$$

$$T_0 = [T_{\mathrm{Load}} \quad T_e \quad T_{\mathrm{MG1}} \quad T_{\mathrm{MG2}} \quad 0 \quad 0 \quad 0 \quad 0]^{\mathrm{T}}$$

$$\dot{\Omega}_0 = [\dot{\omega}_{\mathrm{out}} \quad \dot{\omega}_{\mathrm{eng}} \quad \dot{\omega}_{\mathrm{MG1}} \quad \dot{\omega}_{\mathrm{MG2}} \quad \dot{\omega}_{r1} \quad \dot{\omega}_{c2} \quad F_1 \quad F_2]^{\mathrm{T}}$$

2.2.2 Step 2: Define the Transition Matrices. Transition matrices M and P are defined according to the clutch engagement. M is initialized as a $4n \times 4n$ identity matrix, the same dimension as A_0. When the ith PG node is connected with the jth PG node, without losing generality, assuming $i < j$, the processes shown in Eqs. (6) and (7) are applied to the M matrix. If the clutch is engaged to ground the ith node, ith row = [], which means the row is eliminated. After this step, M becomes a $(4n - q) \times 4n$ matrix, where q is the number of clutches engaged

$$i^{\mathrm{th}}\ \mathrm{row} = i^{\mathrm{th}}\ \mathrm{row} + j^{\mathrm{th}}\ \mathrm{row} \tag{6}$$

$$j^{\mathrm{th}}\ \mathrm{row} = [] \tag{7}$$

The generation of P is similar to that of M, but only row elimination (Eq. (7)) is applied. After this step, P also becomes a $(4n - q) \times 4n$ matrix. M and P matrices are used to obtain the dynamics of the system after clutch engagement, as shown in the following equations:

$$A = MA_0M^{\mathrm{T}}, \quad T = MT_0, \quad \dot{\Omega} = P\dot{\Omega}_0 \tag{8}$$

$$A\dot{\Omega} = T \tag{9}$$

Note that since three power components (engine, MG1, and MG2) are implemented in the powertrain system, the system's DOF must be within the range of one to three so that the vehicle is controllable and drivable. For each nonredundant clutch engagement, 1DOF is reduced. Therefore, the total number of clutches q to be engaged is within the range of $[2n - 3, 2n - 1]$.

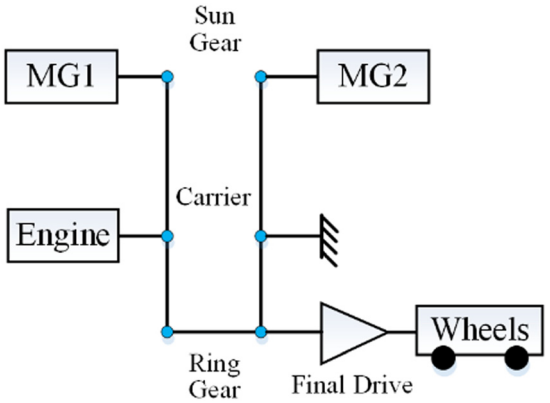

Fig. 3 The lever diagram of THS-II

2.2.3 Step 3: Formulate the Dynamics of the System. The dynamic matrix A of the powertrain system with clutch engagement is generated through Eq. (8). The system dynamics of a certain mode can be represented in Eq. (9). As an example, Eqs. (10) and (11) show the equations of the THS-II powertrain system depicted in Fig. 3

$$M=\begin{bmatrix}1&0&0&0&1&0&0&0\\0&1&0&0&0&0&0&0\\0&0&1&0&0&0&0&0\\0&0&0&1&0&0&0&0\\0&0&0&0&0&0&1&0\\0&0&0&0&0&0&0&1\end{bmatrix},\quad P=\begin{bmatrix}1&0&0&0&0&0&0&0\\0&1&0&0&0&0&0&0\\0&0&1&0&0&0&0&0\\0&0&0&1&0&0&0&0\\0&0&0&0&0&0&1&0\\0&0&0&0&0&0&0&1\end{bmatrix} \tag{10}$$

$$A=\begin{bmatrix}I_{\text{out}}+I_{r2}+I_{r1}&0&0&0&-R_1&-R_2\\0&I_e+I_{c1}&0&0&R_1+R_2&0\\0&0&I_{\text{MG1}}+I_{s1}&0&-S_1&0\\0&0&0&I_{\text{MG2}}+I_{s2}&0&-S_2\\-R_1&R_1+R_2&-S_1&0&0&0\\-R_2&0&0&-S_2&0&0\end{bmatrix},\quad T=\begin{bmatrix}T_{\text{Load}}\\T_e\\T_{\text{MG1}}\\T_{\text{MG2}}\\0\\0\end{bmatrix},\quad \dot{\Omega}=\begin{bmatrix}\dot{\omega}_{\text{out}}\\\dot{\omega}_e\\\dot{\omega}_{\text{MG1}}\\\dot{\omega}_{\text{MG2}}\\F_1\\F_2\end{bmatrix} \tag{11}$$

2.3 Mode Screening. With clutches, multiple modes can be achieved. If the vehicle cannot be powered by any powertrain component in a mode, it is defined as an infeasible mode. For modes with identical dynamic equations, one is kept and the rest are deemed redundant. Distinguishing redundant mode is important for simulation speed in the optimization process later on. In this section, the process and steps to identify and eliminate infeasible and redundant modes are described.

2.3.1 Step 1: Constructing the A^* Matrix. The A matrix is inverted to obtain the dynamic equations that relate inputs to state derivatives. For a controllable powertrain system (i.e., the speed of each PG node can be controlled), the A matrix is always invertible. At the same time, not every element of the A^{-1} matrix is useful. The useful part of A^{-1} is extracted to obtain a final 4×4 matrix A^*, as shown in the equation below

$$\begin{bmatrix}\dot{\omega}_{\text{out}}\\\dot{\omega}_{\text{eng}}\\\dot{\omega}_{\text{MG1}}\\\dot{\omega}_{\text{MG2}}\end{bmatrix}=A^*\begin{bmatrix}T_{\text{load}}\\T_{\text{eng}}\\T_{\text{MG1}}\\T_{\text{MG2}}\end{bmatrix} \tag{12}$$

In order to construct the A^* matrix, the last n columns and rows as well as the columns and rows associated with any free node (node with no powertrain component attached) in A^{-1} are eliminated, as they have no impact on the final state equation. There are two cases following the elimination:

$$A^*=A^{-1}[1:4,1:4] \tag{13}$$

(1) If there is no powertrain component collocation (powertrain components are not connected to the same PG node) due to clutch engagement, the A^* matrix is obtained after the elimination process described in the previous paragraph. As the THS-II example is described in Fig. 3, its A^* is shown in Eq. (13).
(2) If there is collocation, the torque coefficients corresponding to the collocated components are duplicated, making the sequence of the coefficients correspond to "output," "engine," "MG1," and "MG2." In addition, since the accelerations of the collocated components are the same, it will lead to identical rows in the A^* matrix. An example of a parallel mode and its A^{-1} and A^* are shown in Fig. 4 and in the below equation

$$A^{-1}=\begin{bmatrix}A_{11}^{\text{inv}}&A_{12}^{\text{inv}}&A_{13}^{\text{inv}}&A_{14}^{\text{inv}}&A_{15}^{\text{inv}}\\A_{21}^{\text{inv}}&A_{22}^{\text{inv}}&A_{23}^{\text{inv}}&A_{24}^{\text{inv}}&A_{25}^{\text{inv}}\\A_{31}^{\text{inv}}&A_{32}^{\text{inv}}&A_{33}^{\text{inv}}&A_{34}^{\text{inv}}&A_{35}^{\text{inv}}\\A_{41}^{\text{inv}}&A_{42}^{\text{inv}}&A_{43}^{\text{inv}}&A_{44}^{\text{inv}}&A_{45}^{\text{inv}}\\A_{51}^{\text{inv}}&A_{52}^{\text{inv}}&A_{53}^{\text{inv}}&A_{54}^{\text{inv}}&A_{55}^{\text{inv}}\end{bmatrix}A^*=\begin{bmatrix}A_{11}^{\text{inv}}&A_{12}^{\text{inv}}&A_{12}^{\text{inv}}&A_{13}^{\text{inv}}\\A_{21}^{\text{inv}}&A_{22}^{\text{inv}}&A_{22}^{\text{inv}}&A_{23}^{\text{inv}}\\A_{21}^{\text{inv}}&A_{22}^{\text{inv}}&A_{22}^{\text{inv}}&A_{23}^{\text{inv}}\\A_{31}^{\text{inv}}&A_{32}^{\text{inv}}&A_{32}^{\text{inv}}&A_{33}^{\text{inv}}\end{bmatrix} \tag{14}$$

2.3.2 Step 2: Refining the A^* Matrix. For each row of A^*, if three of the four elements are zero, the corresponding component has no connection with the other three components (i.e., the rest of the powertrain), then all the elements in the row are set to zero.

If both the first and the second element of the third and fourth row of A^* is zero, then the MGs are neither connected to the engine nor the vehicle, they will not affect the function of the mode, and both the third and fourth row will be set to zero.

2.3.3 Step 3: Define Entries in A^* Matrix. The four rows of the A^* matrix are named as V_{veh}, V_{eng}, V_{MG1}, and V_{MG2}, respectively, and the elements of the V_{veh} row vector are named C_{veh}, C_{eng}, C_{MG1}, and C_{MG2} for later reference.

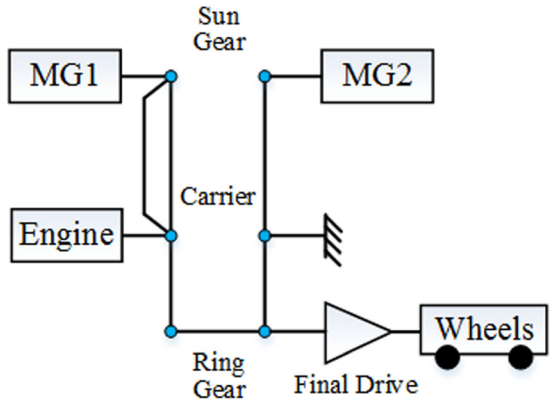

Fig. 4 An example of a parallel mode in THS-II configuration

If the first row of A^* is zero, the vehicle output is not affected by any powertrain component, making it infeasible (not drivable). In addition, vehicle modes with identical A^* matrices are deemed identical.

2.4 Mode Classification. All feasible modes are classified into 14 mode types, as shown in Table 1, which present all possible mode types when one engine, one output shaft, and two MGs are assigned, regardless of the number of PGs.

2.4.1 Step 1: Determine the System DOF. Since each row of the A^* matrix represents the relationship between the torque input and a component's acceleration, rank reduction means that the acceleration of some component can be represented as a linear combination of the accelerations of other components. The DOF of the mode are the same as rank (A^*), which cannot be more than three.

2.4.2 Step 2: Formulate Auxiliary Matrices. Six other matrices are needed for the rank analysis: $M_{VE}=[V_{veh};\ V_{eng}]$, $M_{VMG1}=[V_{veh};\ V_{MG1}]$, $M_{VMG2}=[V_{veh};\ V_{MG2}]$, $M_{EMG1}=[V_{eng};\ V_{MG1}]$, $M_{EMG2}=[V_{eng};\ V_{MG2}]$, and $M_{MG1MG2}=[V_{MG1};\ V_{MG2}]$. The ranks of these matrices are denoted as r_{VE}, r_{VMG1}, r_{VMG2}, r_{EMG1}, r_{EMG2}, and r_{MG1MG2}, and they are used for mode classification, as shown in Table 1.

The SIMULINK diagram of a general multimode HEV powertrain system is shown in Fig. 5, which consists of four parts: the transmission system, the engine system, the electric system, and the supervisory control system. The transmission system is modeled by the procedure proposed in this section; the engine and electric system are modeled by lookup tables [30,31], while the battery model is an equivalent circuit with an open circuit voltage plus internal resistance [13].

3 Enhanced PEARS Algorithm

In general, when assuming that minimum fuel consumption is the goal of optimal control, the problem of multimode HEVs can be defined as in Eq. (15), where the engine speed ω_e, MG1 speed ω_{MG1}, MG2 speed ω_{MG2}, engine torque T_e, MG1 torque T_{MG1}, MG2 torque T_{MG2}, and the operating Mode can be used to determine the fuel consumption

$$\begin{cases} J=\int_{t_0}^{t_f} L(\omega_e,\omega_{MG1},\omega_{MG2},T_e,T_{MG1},T_{MG2},\text{Mode},t)dt \\ \text{subject to :} \\ \text{SOC}(t_0)=\text{SOC}(t_f) \\ \dot{\text{SOC}}=f(\text{SOC},\omega_e,\omega_{MG1},\omega_{MG2},T_e,T_{MG1},T_{MG2},\text{Mode}) \\ \text{SOC}_{\min}\le \text{SOC}\le \text{SOC}_{\max} \\ T_{e_{\min}}\le T_e\le T_{e_{\max}} \\ T_{MG1_{\min}}\le T_{MG1}\le T_{MG1_{\max}} \\ T_{MG2_{\min}}\le T_{MG2}\le T_{MG2_{\max}} \\ \omega_{e_{\min}}\le \omega_e\le \omega_{e_{\max}} \\ \omega_{MG1_{\min}}\le \omega_{MG1}\le \omega_{MG1_{\max}} \\ \omega_{MG2_{\min}}\le \omega_{MG2}\le \omega_{MG2_{\max}} \\ \text{Mode}\in \text{Mode}_{\text{available}} \end{cases} \tag{15}$$

where $L(\omega_e,\omega_{MG1},\omega_{MG2},T_e,T_{MG1},T_{MG2})$ is the rate of fuel consumption of the engine, and SOC is the battery state-of-charge, which is determined by the battery model [13]. Moreover, the torque and speed of the powertrain components are restricted by their operating constraints. The available modes are dependent on each specific design.

To solve this deterministic optimal control problem, the PEARS method has recently been developed and been found to be up to 10,000 times faster than DP [28]. This new methodology can be applied to multiple PG hybrid powertrains. The problem in the previous PEARS was that the mode shift sequence was dependent on the relative power-weighted efficiency (PE) among different modes and on battery energy consumption, which did not consider mode shift feasibility and the mode shift sequence was not optimal. In this paper, DP is applied to determine the mode shift, while other controls are determined by the PEARS algorithm. A comparison between the optimization results of this enhanced PEARS algorithm (PEARS$^+$) and DP will be presented and discussed.

Table 1 Mode types and criteria

	Mode type	Criteria
1	Series mode	$\text{DOF}=2$, $C_{eng}=0$, $V_{eng}\neq 0$, $C_{MG1}C_{MG2}=0$, $C_{MG1}^2+C_{MG2}^2\neq 0$
2	Compound split (3DOF)	$\text{DOF}=3$
3	Compound split (2DOF)	$\text{DOF}=2$, $C_{eng}\neq 0$, $C_{MG1}C_{MG2}\neq 0$, $r_{VMG1}=2$, $r_{VE}=2$, $r_{VMG2}=2$, $r_{EMG1}=2$, $r_{EMG2}=2$
4	Input split	$\text{DOF}=2$, $C_{eng}\neq 0$, $r_{VMG1}\,r_{VMG2}=2$, $C_{MG1}C_{MG2}\neq 0$
5	Output split	$\text{DOF}=2$, $C_{eng}\neq 0$, $r_{EMG1}\,r_{EMG2}=2$, $C_{MG1}C_{MG2}\neq 0$
6	Parallel with EVT (engine + 1MG)	$\text{DOF}=2$, $C_{eng}\neq 0$, $C_{MG1}\,C_{MG2}=0$, $C_{MG1}^2+C_{MG2}^2\neq 0$
7	Parallel with EVT (engine + 2MGs in serial)	$\text{DOF}=2$, $C_{eng}\neq 0$, $C_{MG1}C_{MG2}\neq 0$, $r_{MG1MG2}=1$
8	Engine only (fixed gear)	$\text{DOF}=1$, $C_{eng}\neq 0$ $C_{MG1}^2+C_{MG2}^2=0$
9	Parallel with fixed gear (engine + 2MGs, 2DOF)	$\text{DOF}=2$, $C_{eng}\neq 0$ $r_{VE}=1$, $C_{MG1}C_{MG2}\neq 0$
10	Parallel with fixed gear (engine + 2MGs, 1DOF)	$\text{DOF}=1$, $C_{eng}\neq 0$ $C_{MG1}C_{MG2}\neq 0$
11	Parallel with fixed gear (engine + 1MG, 1DOF)	$\text{DOF}=1$, $C_{eng}\neq 0$ $C_{MG1}\,C_{MG2}=0$, $C_{MG1}^2+C_{MG2}^2\neq 0$
12	EV (2MGs, 2DOF)	$\text{DOF}=2$, $C_{eng}=0$, $V_{eng}(2)=0$
13	EV (2MGs, 1DOF)	$\text{DOF}=1$, $C_{eng}=0$, $V_{eng}(2)=0$ $C_{MG1}C_{MG2}\neq 0$
14	EV (1MG, 1DOF)	$\text{DOF}=1$, $C_{eng}=0$, $V_{eng}(2)=0$ $C_{MG1}\,C_{MG2}=0$, $C_{MG1}^2+C_{MG2}^2\neq 0$

3.1 The PEARS$^+$ Algorithm. The process of the PEARS$^+$ method is presented in Fig. 6 and described below. Details are laid out in steps.

3.1.1 Step 1: Target Cycle Analysis. The target drive cycle is discretized into a two-dimensional table with the X and Y axes being vehicle speed and torque demand, respectively. The table entries represent the probability density of the cells. The cells are referred to as the speed and torque cell (STC) in the subsequent discussion. The reason we choose vehicle torque demand instead of acceleration in Ref. [28] is that then the road grade can be considered without adding another input dimension when discretizing the target cycle.

3.1.2 Step 2: Determine Efficiency for Each Mode. The PE for every mode in each STC is examined. The 14 types of modes are separated into two categories depending on whether the engine is operational or not: EV modes and hybrid modes (where the engine-only operation is treated as a special case of hybrid modes).

3.1.2.1 Step 2.1: Determine EV modes efficiency. The efficiency of the EV modes is described by Eq. (16), where P_{EV}^{loss} includes both battery loss and electric-drive loss and P_{EV}^{in} refers to the power flowing into the system. In the driving scenario, P_{EV}^{in} is the battery power. In the braking case, it is regenerative braking power. Note that friction braking augments regenerative braking, when the latter alone cannot satisfy the driver's demand. For modes with 1DOF, all possible torque combinations (T_{MG1} and T_{MG2}) are compared and the best efficiency is recorded. For modes with 2DOF, not only the torque combination but also the speed combination (ω_{MG1} and ω_{MG2}) is examined. The best possible efficiency of each mode is calculated from Eq. (17). The efficiency of infeasible MG operation (i.e., infeasible MG speed or

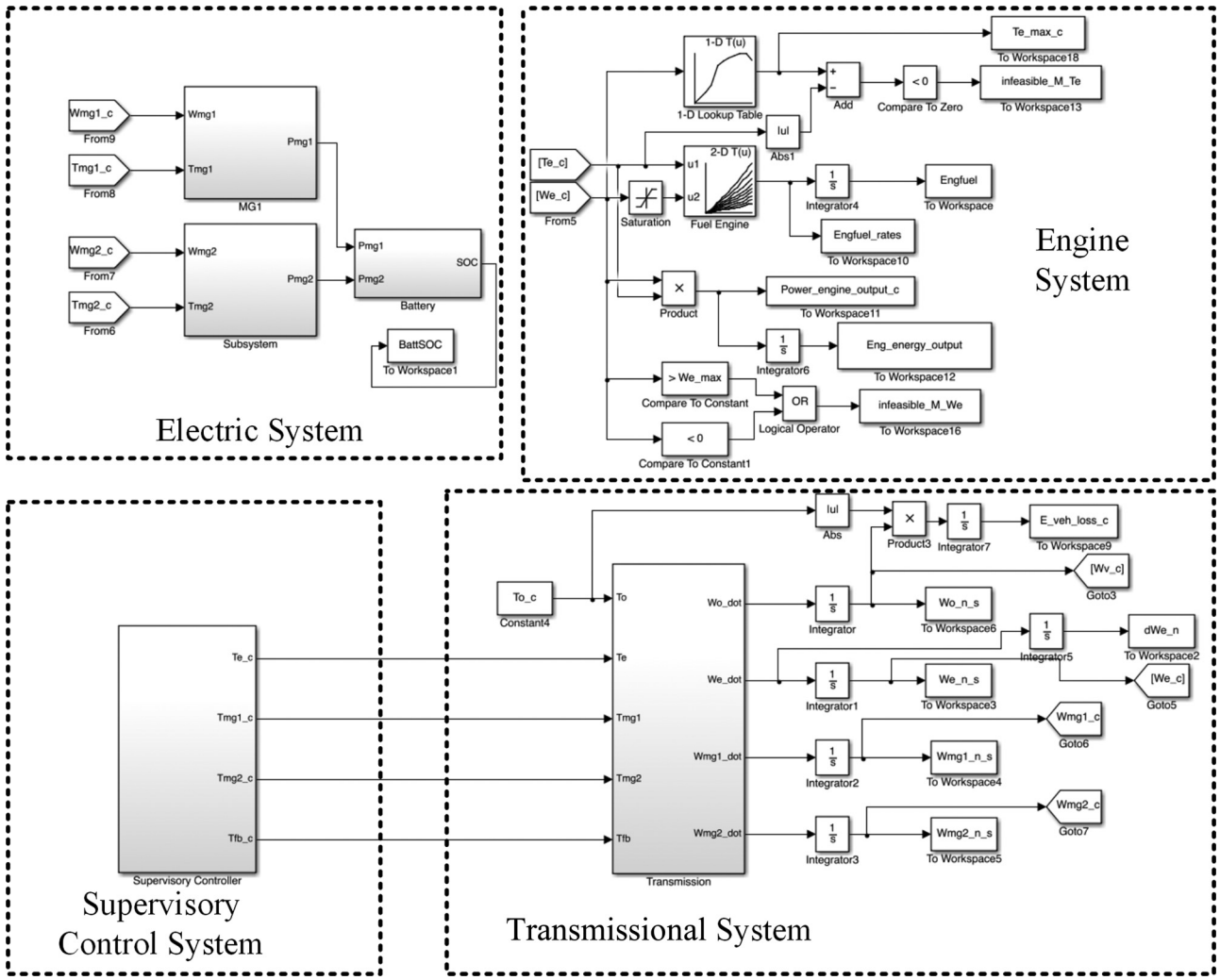

Fig. 5 The SIMULINK diagram of a general multimode HEV powertrain system

torque) will be penalized with zero and the control with the highest efficiency is then selected as the optimal control for each mode in each STC. Meanwhile, the corresponding battery energy consumption will be recorded

$$\eta_{\mathrm{EV}} = 1 - \frac{P_{\mathrm{EV}}^{\mathrm{loss}}}{P_{\mathrm{EV}}^{\mathrm{in}}} \tag{16}$$

$$\eta_{\mathrm{EV}}{}^{*}|_{\omega_{\mathrm{out}},\dot{\omega}_{\mathrm{out}}} = \max[\eta_{\mathrm{EV}}(T_{\mathrm{MG1}}, T_{\mathrm{MG2}})]|_{\omega_{\mathrm{out}},\dot{\omega}_{\mathrm{out}}} \tag{17}$$

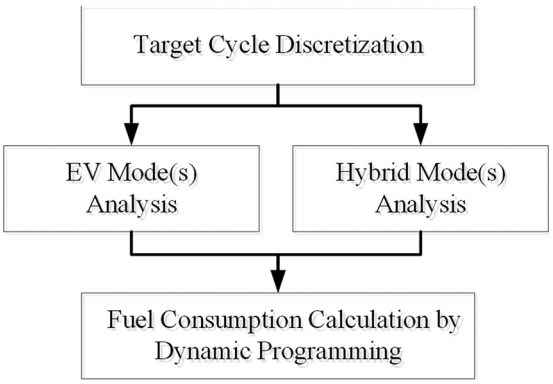

Fig. 6 The PEARS $^{+}$ process

3.1.2.2 Step 2.2: Determine hybrid modes efficiency. Two possible power sources for the hybrid modes are the engine and the battery. In general, the power can be divided into four parts as shown in Table 2, where $P_{e\_1}+P_{e\_2}+P_{e\_3}$ is the total engine power, and P_{batt} is the battery power consumed. Figure 7 describes the power flow paths, where μ is a flag indicating whether or not the battery assist is on.

The PE is calculated in Eq. (18), where P_{fuel} is the rate of fuel energy injected, and subscripts G and M denote the generator (when the power is negative) and the motor (when the power is positive or zero). $\eta_{e\_\max}$, $\eta_{G\_\max}$, and $\eta_{M\_\max}$ represent the highest efficiency of the engine, generator, and the motor. Since engine efficiency is much lower than that of the electrical system, normalization must be used; otherwise, the engine operation will hardly be selected.

Similar to the EV cases, all torque and speed combinations will be examined. The control with the highest efficiency is then

Table 2 Power flows in the hybrid powertrain

Power flows	Description
$P_{\mathrm{e\_1}}$	Engine power flows through the generator to the battery
$P_{\mathrm{e\_2}}$	Engine power flows through the generator to the motor
$P_{\mathrm{e\_3}}$	Engine power directly flows to the final drive
P_{batt}	Battery power

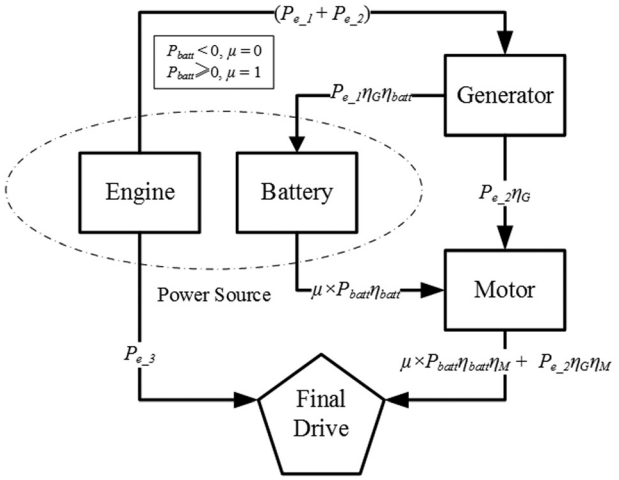

Fig. 7 Power flow in the hybrid mode

selected for each hybrid mode in each STC. Meanwhile, the corresponding battery energy and fuel consumption are recorded

$$\eta_{\text{Hybrid}}(\omega_e, T_e) = \frac{P_{e_1}\eta_G\eta_{\text{batt}}/(\eta_{e_{\max}}\eta_{G_{\max}})}{P_{\text{fuel}}+\mu P_{\text{batt}}} + \frac{P_{e_2}\eta_G\eta_M/(\eta_{e_{\max}}\eta_{G_{\max}}\eta_{M_{\max}})}{P_{\text{fuel}}+\mu P_{\text{batt}}} + \frac{P_{e_3}/\eta_{e_{\max}}+\mu P_{\text{batt}}\eta_{\text{batt}}\eta_M/\eta_{M_{\max}}}{P_{\text{fuel}}+\mu P_{\text{batt}}} \tag{18}$$

$$\eta_{\text{Hybrid}}{}^*|_{\omega_{\text{out}},\dot{\omega}_{\text{out}}} = \max[\eta_{\text{Hybrid}}(\omega_e, T_e)]|_{\omega_{\text{out}},\dot{\omega}_{\text{out}}} \tag{19}$$

3.1.3 Step 3: Calculate the Optimal Mode Shift With DP. Once the optimal control executions are determined for each mode at each vehicle STC, the next step is to determine the mode to be used during the drive cycle.

The states and controls of the DP problem are shown in Table 3. The first state is battery energy consumption, which is calculated from step 2; the second state and control are both operating modes. Note that the mode is a state because the cost function includes the mode shift penalty.

The cost function and constraint of the DP problem are described in Eqs. (20) and (21): the optimization objective is to minimize fuel consumption while keeping the mode shift number and final delta SOC small

$$J = \min\left[\sum_{t=1}^{N}(L_t + \gamma_1\Delta\omega_e^2 + \gamma_2\Delta\omega_{\text{MG1}}^2 + \gamma_3\Delta\omega_{\text{MG2}}^2) + \alpha(\text{SOC}_{\text{desired}} - \text{SOC}_N)^2\right] \tag{20}$$

Subject to

$$\text{SOC}_{\min} \leq \text{SOC} \leq \text{SOC}_{\max} \tag{21}$$

where γ_1, γ_2, and γ_3 are the factors to penalize for speed difference, and α is the factor for the equality constraint of the final SOC.

Table 3 The states and controls for PEARS$^+$ DP problem

States and controls	Description
State 1	Battery energy consumption (equivalent to SOC)
State 2	Previous mode
Control 1	Mode selection

Table 4 Parameters of the vehicle used in the case study (based on Prius MY2010)

Component	Parameters
Engine	98 hp at 5200 rpm 105 lbft at 4000 rpm
P_{MG1max} (kW)	42
P_{MG2max} (kW)	60
Final drive ratio	3.2
R_1:S_1	2.6
R_2:S_2	2.63
Vehicle mass (kg)	1450

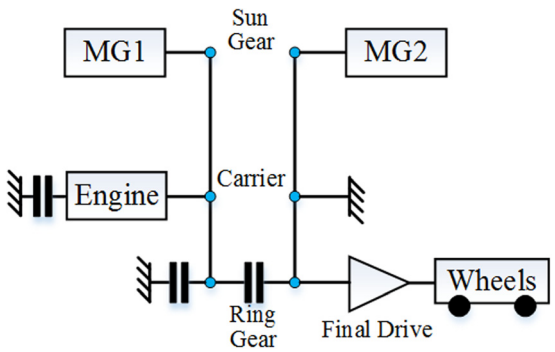

Fig. 8 Lever diagram of the Prius 2010^{++}

Table 5 Operating modes of the Prius 2010^{++}

Mode #	Description
1	EV (1MG, 1DOF)
2	EV (2MGs,1DOF)
3	Series mode
4	Input-split mode

This low-dimension DP problem only takes 15–30 s (depending on the number of modes for the design being studied) to solve for the 1372-s long Federal Urban Driving Schedule (FUDS).

3.2 Comparison Between the PEARS$^+$ and DP. In this subsection, a larger DP problem will be solved to validate the PEARS$^+$ algorithm. A double PG conceptual design named Prius 2010^{++} is adopted, which evolved from Prius^{++} [13] and Prius 2010 (whose parameters are listed in Table 4). The lever diagram in Fig. 8 shows that the Prius2010^{++} augments the Prius 2010 (THS-II, Fig. 3) by adding three clutches; its operating modes are described in Table 5.

In this larger DP problem, all control decisions are solved by DP, and its states and controls are listed in Table 6, which uses the same cost function shown in Eq. (20).

Table 6 States and controls of the traditional DP problem

States and controls	Description
State 1	Battery SOC
State 2	Engine speed
State 3	Mode
Control 1	Torque of engine
Control 2	Torque of MG1
Control 3	Mode

Table 7 Optimization results of PEARS$^+$ and traditional DP

Method	Fuel consumption (MPG)/difference				Computation time (s)[a]	
	FUDS		HWFET		FUDS	HWFET
PEARS$^+$	69.9	3.1%	56.8	3.2%	30	17
DP	72.1		58.7		301,840	168,520

[a]The results are based on a desktop computer with Intel Xeon E5-1620 (3.7GHz) and 32 GB RAM.

Both FUDS and the highway fuel economy test (HWFET) cycles are simulated, and the state/control trajectories for both methods in FUDS cycle are shown in Table 7 and Figs. 9 and 10. Note that the vehicle is running on the charge-sustaining drive, which means the final SOC must be the same as the initial SOC.

From Table 7, it can be observed that PEARS$^+$ results are near-optimal, all while being much faster to compute. In addition, the PEARS$^+$ results are also qualitatively similar to DP. The difference in fuel economy is less than 3.5%, but the PEARS + method is about 10,000 times faster than the traditional DP, making it feasible for fast prototype design and sizing, even for on-board model predictive control if a short future driving profile can be forecast. In Sec. 4, we use PEARS$^+$ as the optimization approach for generating energy management strategies for the candidate designs.

4 Case Study

The case study presented here combines the modeling procedure introduced in Sec. 2 and PEARS$^+$ described in Sec. 3 to find optimal and suboptimal designs.

In this study, we only consider cases when two powertrain components are connected to each of the PGs, since having three powertrain components on the same PG will likely lead to very limited operation flexibility. Thus, the number of configurations is $C_4^2P_3^2P_3^2 = 216$. In addition, topologically, the remaining 216 configurations can be classified into two types, depending on whether or not the engine and output shaft are on the same PG, as depicted in Fig. 11. For type (a), there are $C_2^1C_2^1P_3^2P_3^2 = 144$ configurations and for type (b), there are $C_2^1P_3^2P_3^2 = 72$ configurations. The THS-II Drive design, which is used in the current generation of Prius, Camry hybrid, and Highlander hybrid, is an example of category (a) configuration, as shown in Fig. 9.

Due to the large design pool, in this paper, we choose THS-II and use the powertrain components of Prius 2010 in Table 4. In other words, we are only exploring the clutch placement but not the design search in the configuration or the sizing dimension. Searching those dimensions may result in even better designs.

While we start by studying the design cases with all 16 clutches, it is clear that the resulting design only serves as a benchmark and would be difficult to implement in practice. Moreover, inasmuch as we likely do not need all the modes enabled by 16 clutches. In this study, we will further investigate the cases where three clutches and one fixed connection are used because the three clutches may lead to as many as seven different modes, resulting in many feasible and suboptimal designs. In addition, the Chevy Volt uses three clutches, which means it must be feasible in practice.

For double PGs, 16 clutches may have $2^{16} = 65{,}536$ clutch states in theory. After the screening process, for configurations described in Fig. 11(*a*), only 101 feasible and nonredundant modes remain, when the two MGs are treated as different components. Figure 12 shows the distribution of the feasible and

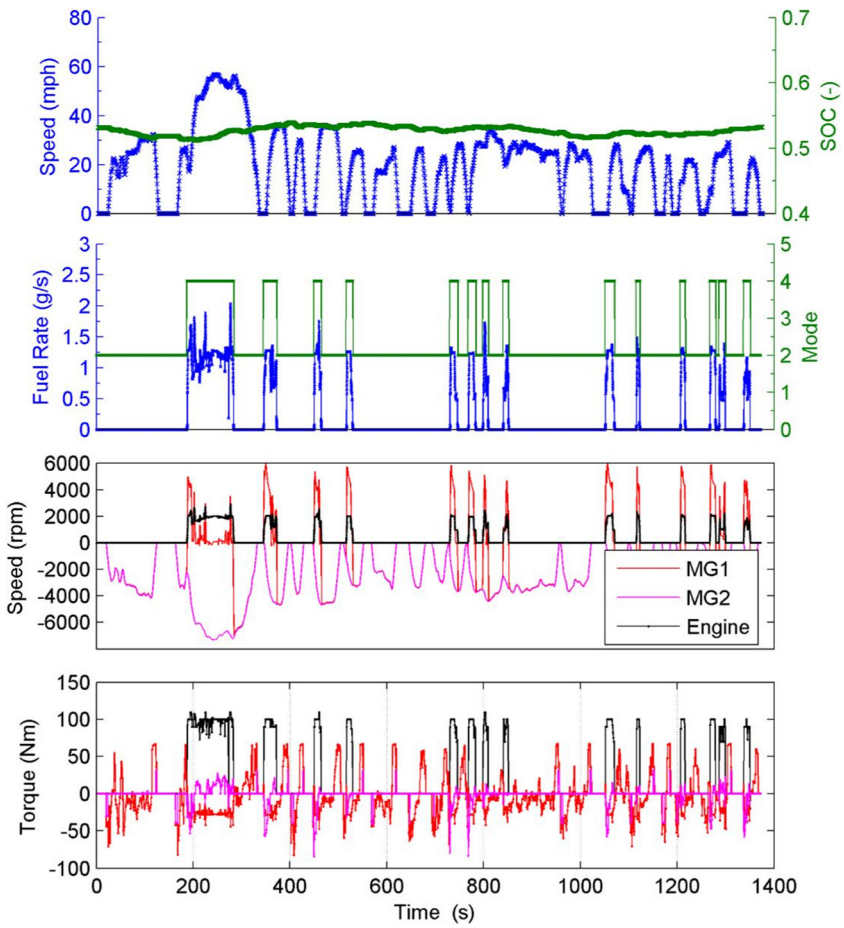

Fig. 9 Trajectories of DP in the FUDS cycle

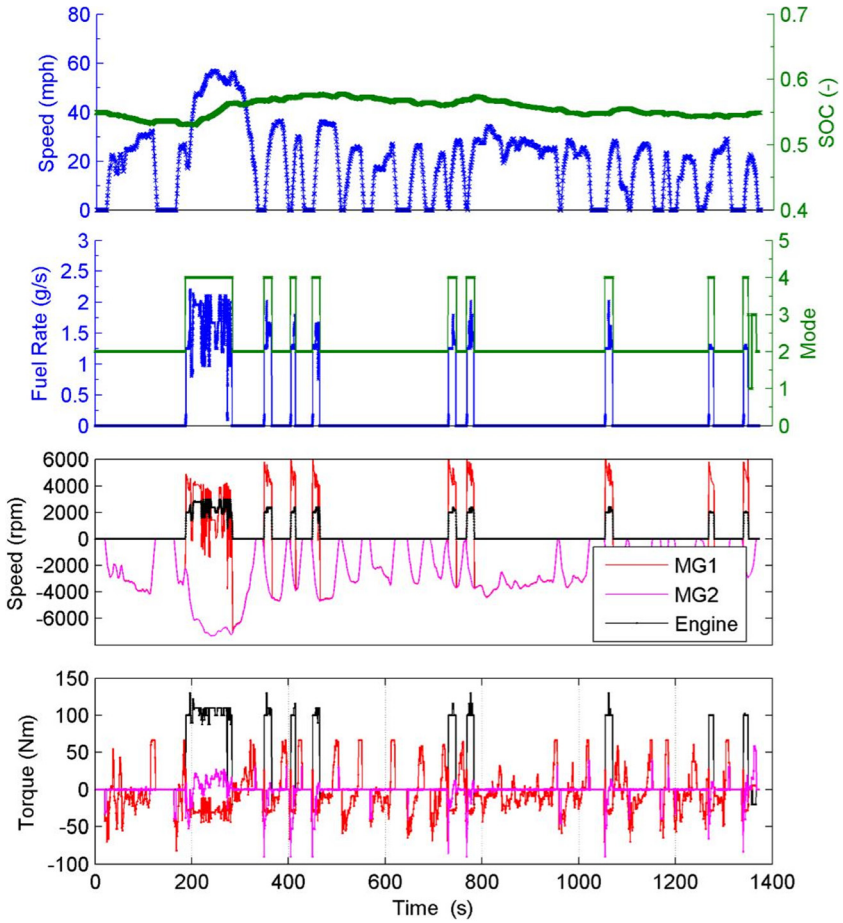

Fig. 10 Trajectories of PEARS$^+$ in the FUDS cycle

nonredundant modes for the configuration used in THS-II and configurations of category (a). The reason all 144 configurations of category (a) have the same number and type of modes is that varying the connection of a node on one PG will only change the relative speed ratio, but not the function of the mode.

4.1 The "Utopian" Design (Adding 16 Clutches). The Utopian design (when all clutches shown in Fig. 2 are used) can shift among all 101 modes. The results serve as the idealized benchmark.

The fuel consumption, selected operating modes, and their frequency in both city and highway cycles are shown in Figs. 13 and 14. It can be observed that the EV modes and hybrid modes are used almost evenly. The power-split mode and parallel mode with fixed-gear are the preferred hybrid modes in city and highway driving, respectively. Even though only five mode types are shown in Fig. 14, about ten different modes are used. To enable all ten modes, ten of the 16 clutches are needed, which is somewhat impractical to implement due to the added cost and system complexity.

4.2 Power-Based Acceleration Analysis. Before applying the PEARS$^+$ algorithm, drivability criteria will be used to screen out designs with undesirable acceleration performance, which helps to focus on the more practical part of the design pool.

To enable such screening, a systematic methodology must be developed to find the optimal mode shift sequence for achieving the best acceleration performance. In this section, a power-based drivability analysis is used.

First, we divide the total vehicle speed interval of [0,60] mph into 30 subintervals with 2 mph increment. In each subinterval, the vehicle speed is assumed to be at the mean value of the interval, and the maximum possible output power of each mode is calculated: for the mode with 1DOF, this is trivial since the maximum power occurs when each power component is generating its maximum torque; for modes with more than 1DOF, the acceleration of the engine will be assumed to be zero for steady-state analysis, and all possible speed combinations will be evaluated, selecting the state and control with the highest power output.

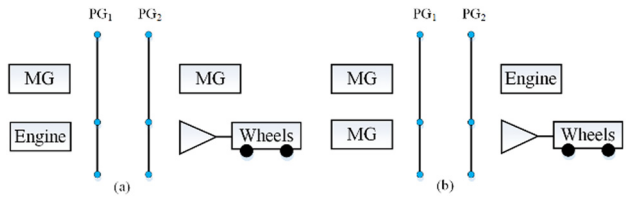

Fig. 11 Two types of configurations

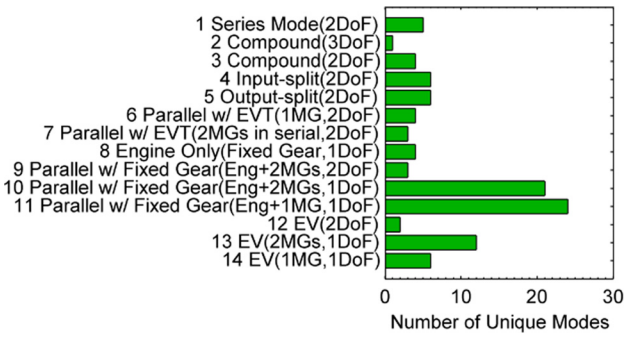

Fig. 12 All feasible and nonredundant modes for the configuration used in Prius 2010, grouped into 14 mode types

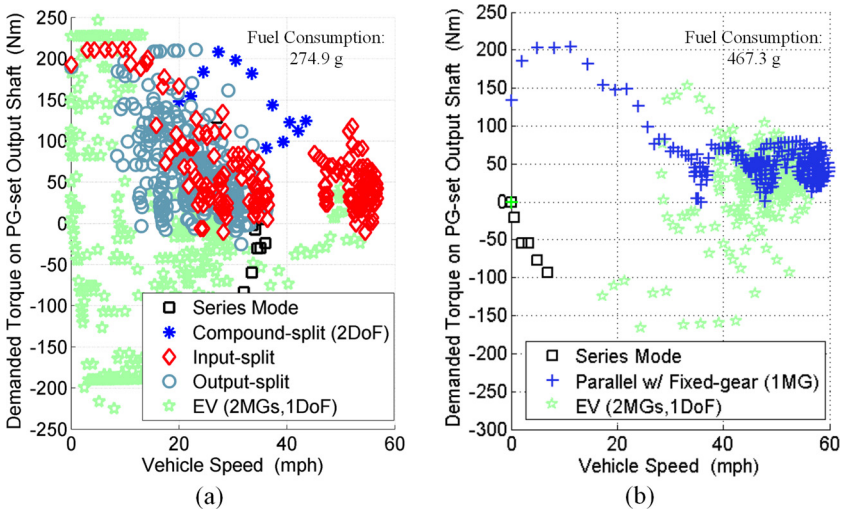

Fig. 13 Optimal modes used in the FUDS and HWFET cycles

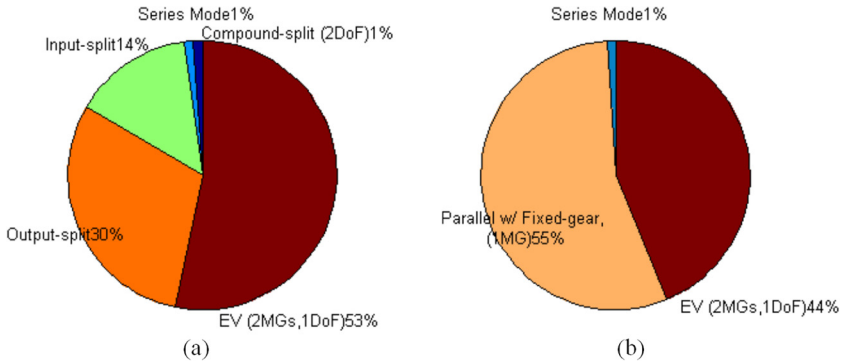

Fig. 14 The mode types and usage frequency (percentage of time each mode type is used) of the Utopian design

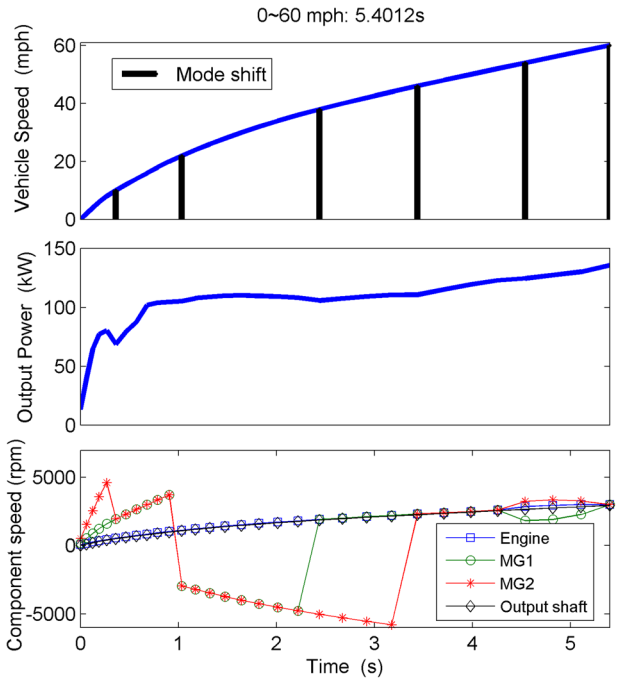

Fig. 15 The mode shift and acceleration profile of the Utopian design

Table 8 The PEARS^{+} optimization result for FUDS and HWFET cycle, respectively

Cycle\design	Fuel consumption (MPG)			
	Prius 2010	Prius 2010^{++}	Best with three clutches	Utopian
FUDS	67.6	69.9	73.3	73.8
HWFET	56.2	56.8	59.2	59.9

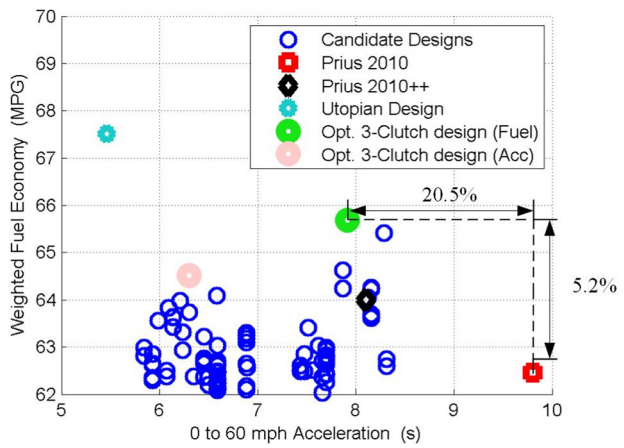

Fig. 16 Optimization results comparing three-clutch designs and the benchmarks

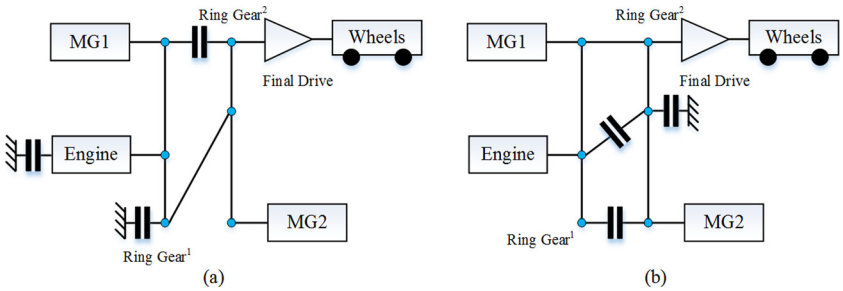

Fig. 17 Lever diagrams of the two suboptimal designs selected in Fig. 16

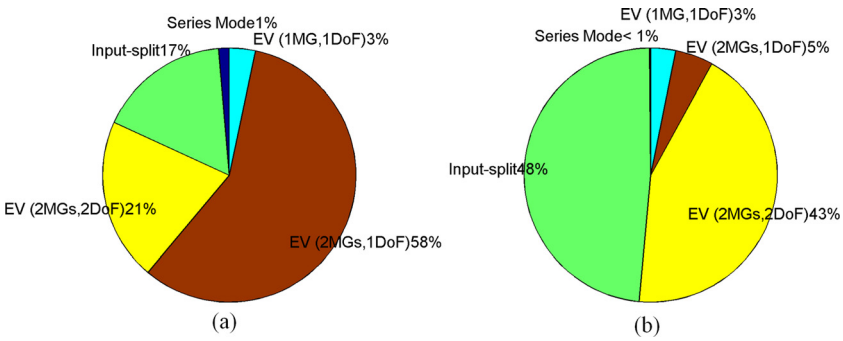

Fig. 18 The mode types and usage frequency of the suboptimal design for fuel economy

With this methodology, the mode selection, component state, and control profile for the Utopian design are generated, as shown in Fig. 15. Note that the smoothness and time for mode shifts are not considered in this paper.

4.3 Configurations With Three Clutches and One Fixed Connection. For practical considerations, we consider the suboptimal cases when only three clutches and one fixed connection are allowed, which leads to $C_{16}^{1}\,C_{15}^{3} = 7280$ different "designs." Each combination may have up to seven different modes. In the following context, "a design" refers to one such particular combination of clutch allocation for the THS-II configuration. The launching performance constraint is set at 8.5 s for 0–60 mph acceleration. After the drivability screening procedure, 308 of the 7280 designs were determined to be feasible and advanced to the fuel economy evaluation step. Because DP is computationally too expensive for solving the optimization problem with such a large design space, we will use PEARS+ to identify the optimal design.

The optimization results from PEARS^{+} for FUDS and HWFET cycle are shown in Table 8. It can be found that, even when only three clutches and one fixed connection are used, similar fuel economy can be achieved, compared to the Utopian design.

It could be that the best design for the FUDS cycle may not be the same as the one for the HWFET cycle. To reflect a balanced fuel economy performance in both city and highway driving, we use a weighted fuel economy following the Environmental Protection Agency's practice of using 55% weight on the city cycle (FUDS) and 45% on the highway cycle (HWFET).

Out of the 7280 designs, 177 achieve better performance in both fuel economy and drivability than the benchmark Prius 2010, as shown in Fig. 16. We highlight two suboptimal designs, one for better fuel economy (highlighted in green), and one for better launching performance (highlighted in pink). Compared with the original Prius 2010, the fuel economy-focused suboptimal design improves fuel economy and drivability by 5.2% and 20.5%, respectively. Compared with the imagined Prius 2010^{++} (not available on production vehicles), the best three-clutch fuel economy-focused design is better by about 2.6% and 2.3%, respectively. If we are to put more emphasis on drivability, the suboptimal design highlighted in pink can be an alternative for a more balanced design, which is at the corner of the Pareto front (with an improvement of 3.3% and 35.7% on drivability and launching, respectively, compared to the Prius 2010). The lever diagrams of the two suboptimal designs are shown in Fig. 17. Note that these two designs are just for the specific powertrain parameters in this study, the suboptimal designs may vary with different powertrain parameters (i.e., R:S, FR, etc.).

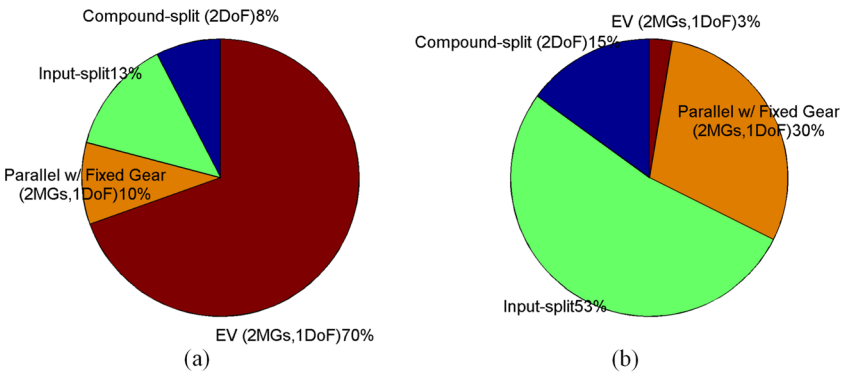

Fig. 19 The mode types and usage frequency of the suboptimal design for drivability

From the mode selection of the Utopian design and the two suboptimal three-clutch designs (Figs. 18 and 19), we can see that EV modes are very frequently used in both city and highway driving. When the engine is turned on (for charge sustaining), the most frequently used modes can be input-split, parallel, or compound-split mode types. We believe the best mode selection depends on configuration, component sizes, and the drive cycle. Having clutches and multiple-modes to add to the flexibility in mode selection is definitely a valuable addition.

It should be noted that, in this research, component sizing and powertrain parameters have not been optimized. One can adopt this similar process to study the sizing problem. The main purpose of the case study was to demonstrate the potential of this proposed design methodology. The preferred modes and winning design will likely vary with the selected powertrain configuration and component sizes.

It should also be noted that losses such as clutch friction loss and transmission loss are not considered in this design procedure. More sophisticated model will be used in the next design procedure, once the final design candidates are identified.

5 Conclusion

In this research, an automated modeling method and a fast suboptimal control procedure are developed that can be used to explore a large number of power-split configurations with PGs and clutches. We also developed methods to identify and eliminate infeasible and redundant modes and established a power-based acceleration analysis algorithm.

The proposed design procedure was applied to the THS-II configuration used in the Prius 2010 model year. The goal was to determine whether clutches should be added to improve launching performance and fuel economy, and if so, where they should be located. We analyzed both a Utopian design in which all 16 possible clutches are used, and a more practical scenario, where only three clutches and a fixed connection are allowed. We found 177 designs that achieve better fuel economy and better launching performance than the benchmark THS-II configuration (used in the MY 2010 Prius) using the same engine and electric machines. A fuel economy-focused suboptimal design is better by 5.2% and 20.5% in fuel economy and drivability, respectively. When drivability is emphasized, an alternative design achieves a 35.7% shorter 0–60 acceleration time than the benchmark, yet still improves 3.3% in fuel economy. We should point out that the optimal design may vary with the configurations and component sizes. Thus, the key contribution of this research may be neither the identified suboptimal designs nor a comparison of the performance of multimode HEVs with single-mode HEVs, but rather a systematic design methodology for multimode HEVs.

Acknowledgment

This paper is based upon the work supported by the Department of Energy under Award No. DE-PI0000012. The second author was supported by NSFC under Grant No. 51205228.

References

[1] 2012, "Part II: Environment Protection Agency," *Federal Register*, Vol. 77, pp. 62623–63200.
[2] Mi, C., Masrur, M. A., and Gao, D., 2011, *Hybrid Electric Vehicles: Principles and Applications With Practical Perspectives*, Wiley Online Library, London.
[3] Ehsani, M., Gao, Y., and Emadi, A., 2009, *Modern Electric Hybrid Electric and Fuel Cell Vehicles: Fundamentals, Theory, and Design*, 2nd ed., CRC Press, Boca Raton.
[4] Miler, M., Holmes, A., Conlon, B., and Savagian, P., 2011, "The GM 'Voltec' 4ET50 Multi-Mode Electric Transaxle," SAE Int., **4**(1), pp. 1102–1114.
[5] 2010, "Alternative Fuels and Advanced Vehicles Data Center, Data, Analysis, and Trends: Vehicle—HEV Sales by Model," Last accessed Sept. 20, 2013, http://www.afdc.energy.gov/afdc/data/vehicles.html
[6] Schmidt, M. R., 1999, "Two-Mode, Compound-Split Electro-Mechanical Vehicular," U.S. Patent No. 5,931,757.
[7] Rahman, K., and Anwar, M., 2011, "The Voltec 4ET50 Electric Drive System," SAE Int., **4**(1), pp. 323–337.
[8] Si, B., 2011, "Reconfiguration Hybrid Powertrain," U.S. Patent No. 0,319,211.
[9] Seo, K., and Yang, H., 2012, "Powertrain for Hybrid Vehicle," U.S. Patent No. 8,147,367.
[10] Muta, K., Yamazaki, M., and Tokieda, J., 2004, "Development of New-Generation Hybrid System THS II—Drastic Improvement of Power Performance and Fuel Economy," SAE Technical Paper No. 2004-01-0064.
[11] Bucknor, N. K., Hendrickson, J. D., and Raghavan, M., 2007, "Electrically Variable Transmission Having Two Planetary Gear Sets With One Fixed Interconnection," U.S. Patent No. 7,198,373.
[12] Si, B., 2011, "Dual Mode Input Split Compound Split Configuration EPPV Transmission," U.S. Patent No. 8,075,435.
[13] Zhang, X., Li, C.-T., Kum, D., and Peng, H., 2012, "Prius+ and Volt−: Configuration Analysis of Power-Split Hybrid Vehicles With a Single Planetary Gear," IEEE Trans. Veh. Technol., **61**(8), pp. 3544–3552.
[14] Liu, J., and Peng, H., 2010, "A Systematic Design Approach for Two Planetary Gear Split Hybrid Vehicles," Veh. Syst. Dyn., **48**(11), pp. 1395–1412.
[15] Li, C.-T., and Peng, H., 2010, "Optimal Configuration Design for Hydraulic Split Hybrid Vehicles," American Control Conference, Baltimore, MD, pp. 5812–5817.
[16] Hermance, D., 1999, "Toyota Hybrid System," SAE TOPTEC Conference, Albany, NY.
[17] Jalil, N., Kheir, N., and Salman, M., 1997, "A Rule-Based Energy Management Strategy for a Series Hybrid Vehicle," American Control Conference, Albuquerque, NM, June 4–6, pp. 689–693.
[18] Pagalelli, G., Delprat, S., Guerra, T., Rimaux, J., and Santin, J., 2002, "Equivalent Consumption Minimization Strategy for Parallel Hybrid Powertrains," 55th IEEE Vehicular Technology Conference, pp. 2076–2081.
[19] Sciarretta, A., Back, M., and Guzzella, L., 2004, "Optimal Control of Parallel Hybrid Electric Vehicles," IEEE Trans. Veh. Technol., **12**(3), pp. 352–363.
[20] Delprat, S., Lauber, J., Guerra, T. M., and Rimaux, J., 2004, "Control of a Parallel Hybrid Powertrain: Optimal Control," IEEE Trans. Veh. Technol., **53**(3), pp. 872–881.
[21] Delprat, S., Guerra, T. M., and Rimaux, J., 2002, "Control Strategies for Hybrid Vehicles: Optimal Control," 56th IEEE Vehicular Technology Conference, Vancouver, BC, Canada, pp. 1681–1685.
[22] Kim, N., Cha, S., and Peng, H., 2010, "Optimal Control of Hybrid Electric Vehicles Based on Pontryagin's Minimum Principle," IEEE Trans. Control Syst. Technol., **19**(5), pp. 1279–1287.
[23] Lin, C.-C., Peng, H., Grizzle, J., and Kang, J.-M., 2003, "Power Management Strategy for a Parallel Hybrid Electric Truck," IEEE Trans. Control Syst. Technol., **11**(6), pp. 839–849.
[24] Liu, J., and Peng, H., 2006 "Control Optimization for a Power-Split Hybrid Vehicle," American Control Conference, Minneapolis, MN, pp. 466–471.
[25] Murgovski, N., Johannesson, L., Sjoberg, J., and Egardt, B., 2012, "Component Sizing of a Plug-In Hybrid Electric Powertrain Via Convex Optimization," Mechatronics, **22**(1), pp. 106–120.
[26] Hu, X., Murgovski, N., Johannesson, L., and Egardt, B., 2013, "Energy Efficiency Analysis of a Series Plug-In Hybrid Electric Bus With Different Energy Management Strategies and Battery Sizes," Appl. Energy, **111**, pp. 1001–1009.
[27] Hu, X., Murgovski, N., Johannesson, L., and Egardt, B., 2014, "Comparison of Three Electrochemical Energy Buffers Applied to a Hybrid Bus Powertrain With Simultaneous Optimal Sizing and Energy Management," IEEE Trans. Intell. Transp. Syst., **15**(3), pp. 1193–1205.
[28] Zhang, X., Peng, H., and Sun, J., 2015, "A Near-Optimal Energy Management Strategy for Rapid Component Sizing of Multimode Power Split Hybrid Vehicles," IEEE Trans. Control Syst. Technol., **23**(2), pp. 609–618.
[29] Benford, H., and Leising, M., 1981, "The Lever Analogy: A New Tool in Transmission Analysis," SAE Paper No. 810102.
[30] Olszewski, M., 2011, "Evaluation of the 2010 Toyota Prius Hybrid Synergy Drive System," Oak Ridge National Laboratory Report.
[31] Kawamoto, N., Naiki, K., Kawai, T., Shikida, T., and Tomatsuri, M., 2009, "Development of New 1.8-Liter Engine for Hybrid Vehicles," SAE Technical Paper No. 2009-01-1061.